RSC Advances

PAPER

View Article Online
View Journal | View Issue

Cite this: *RSC Adv.*, 2018, **8**, 5640

A simple hydrazone as a multianalyte (Cu^{2+}, Al^{3+}, Zn^{2+}) sensor at different pH values and the resultant Al^{3+} complex as a sensor for F^-†

Wei-Na Wu,[a] Hao Wu,[a] Yuan Wang,*[a] Xian-Jie Mao,[a] Bao-Zhong Liu,*[a] Xiao-Lei Zhao,[a] Zhou-Qing Xu,[a] Yun-Chang Fan[a] and Zhi-Hong Xu*[b]

Received 14th September 2017
Accepted 13th January 2018

DOI: 10.1039/c7ra10219d

rsc.li/rsc-advances

A new colorimetric and fluorescence molecular chemosensor based on triazole hydrazone can be used as a multi-probe for selective detection of Al^{3+}, Zn^{2+}, and Cu^{2+} by monitoring changes in the absorption and fluorescence spectral patterns. Results show that Al^{3+} and Zn^{2+} ions can induce remarkable fluorescence enhancement at pH 6.0 and pH 10.0, respectively, while the addition of Cu^{2+} ions leads to a significant UV-visible absorption enhancement in the visible range at pH 6.0. In addition, the resultant Al^{3+} complex could act as an 'on–off' fluorescence sensor for F^-. The fluorescence sensor was also used to monitor intracellular Al^{3+}, Zn^{2+}, and F^- in Hela cells.

Introduction

Fluorescence methods based on molecular chemosensors are important tools for the recognition of metal ions owing to the operational simplicity and low detection limits.[1,2] A new chemosensor design concept of a 'single sensor for multiple analytes' has been introduced recently.[3] Compared to one-to-one analysis methods, a chemosensor with different responses toward multiple metal ions and good bioimaging ability is highly desirable for practical applications.[4]

Aluminum is the most abundant metal element on earth, accounting for about 8% of total mineral components, and it plays an important role in many fields.[5] However, excess aluminum can damage the human nervous system and induce several health hazards.[5,6] The World Health Organization limits Al^{3+} concentration in drinking water to 200 μg L^{-1} (7.41 μM).[7] In general, Al^{3+} prefers hard donor sites (*e.g.*, O and N) in its coordination sphere because of its strong acidity, and the strong hydration of Al^{3+} in aqueous media leads to its weak coordination ability.[8,9] Besides, the detection of Al^{3+} can be easily interfered with by the matrix, leading to limited selectivity and sensitivity.[10–12] Thus, designing a selective and sensitive fluorescence probe for Al^{3+} in aqueous media remains a challenge.

Unlike Al^{3+} ion, Zn^{2+} and Cu^{2+} ions are essential elements in biological systems.[13–16] However, at high concentrations, Zn^{2+}/Cu^{2+} ion could also cause disorders associated with neurodegenerative diseases.[17,18] For fluorescent detection of Zn^{2+}, most of the reported sensors are affected by cross interference of Cd^{2+} owing to their closely related electronic and binding properties.[19,20] On the other hand, excessive Cu^{2+} is harmful to the environment,[21] and colorimetric probes for Cu^{2+} determination are widely used because they can monitor Cu^{2+} both in solution and on test strips, which can be evaluated by the naked eye.[22,23]

It has been noted that Schiff base sensors deserve special attention due to their simplicity, sensitivity, easy operation, and low cost.[15] Although a number of sensors towards two of Cu^{2+}, Al^{3+}, and Zn^{2+} ions have been developed,[5,6,17,23–27] simultaneous selective detection of all three ions by a molecular chemosensor based on a Schiff base scaffold is rarely reported.

Considering the above circumstance, we report here an acylhydrazone derivative **1** (Scheme 1) bearing a triazole ring as a fluorescent turn-on probe toward Al^{3+} and Zn^{2+} ions at different pH values, and also as a colorimetric probe for Cu^{2+} detection. Noticeably, the **1** + Al^{3+} system is able to detect F^- ions by fluorescence quenching, as the resultant metal-probe complex used as secondary sensor is one of the most promising design strategies for the detection of fluoride.[28–30] In addition, the application of the fluorescent probe in living cell image is demonstrated.

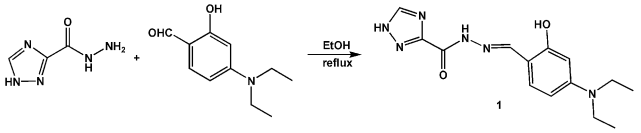

Scheme 1 Synthesis route of the probe **1**.

[a]*College of Chemistry and Chemical Engineering, Henan Key Laboratory of Coal Green Conversion, Henan Polytechnic University, Jiaozuo 454000, P. R. China. E-mail: wangyuan08@hpu.edu.cn; bzliu@hpu.edu.cn*

[b]*Key Laboratory of Chemo/Biosensing and Detection, School of Chemistry and Chemical Engineering, Xuchang University, 461000, P. R. China. E-mail: xuzhihong1980@yahoo.com*

† Electronic supplementary information (ESI) available: ^{1}H NMR ESI-MS spectrum and other additional figures for the probe. CCDC 1541522. For ESI and crystallographic data in CIF or other electronic format see DOI: 10.1039/c7ra10219d

Experimental section

Materials and instrumentation

Solvents and starting materials for syntheses were purchased commercially and used as received. Elemental analyses were carried out on an Elemental Vario EL analyzer. ^{1}H NMR spectra are recorded on a Bruker AV400 NMR spectrometer in DMSO-d_6 solution. The UV spectra were recorded on a Purkinje General TU-1800 spectrophotometer. Fluorescence spectra were determined on a Varian CARY Eclipse spectrophotometer. ESI-MS spectra were obtained on a Bruker Daltonics Esquire 6000 mass spectrometer. Fluorescent images were taken on a Zeiss Leica inverted epifluorescence/reflectance laser scanning confocal microscope. The X-ray diffraction measurement for **1**·0.5H_2O was performed on a Bruker SMART APEX II CCD diffractometer equipped with a graphite monochromatized MoKα radiation (λ = 0.71073 Å) by using ϕ-ω scan mode. Semi-empirical absorption correction was applied to the intensity data using the SADABS program.[31] The structure was solved by direct methods and refined by full matrix least-square on F^2 using the SHELXTL-97 program.[32] All non-hydrogen atoms were refined anisotropically. All H atoms were positioned geometrically and refined using a riding model.

Synthesis of 1

A quantity of 1,2,4-triazole-3-carbohydrazide (1.27 g, 10 mmol) was added to an EtOH solution (50 mL) containing 4-(diethylamino)-2-hydroxybenzaldehyde (1.93 g, 10 mmol). The mixture was refluxed for 3 h with two drops of acetic acid. After cooling to room temperature, the separated solid was filtered, washed with EtOH, and then dried in air. Yield 79%. Anal. calc. for $C_{15}H_{19}N_5O_2$: C, 59.79; H, 6.36; N, 23.24. Found: C, 59.89; H, 6.48; N, 23.11%. ^{1}H NMR (400 MHz, DMSO-d_6), δ (ppm): 14.79 (s, 1H, OH), 12.13 (s, 1H, NH), 11.41 (s, 1H, NH-triazole), 8.62 (s, 1H, CH-triazole), 8.54 (s, 1H, CH=N), 7.14–7.16 (d, 1H, aryl-H), 6.26–6.29 (dd, 1H, aryl-H), 6.12–6.13 (d, 1H, aryl-H), 3.33–3.39 (q, 4H, 2CH_2), 1.09–1.12 (t, 6H, 2CH_3). ESI-MS: m/z = 303.1804 for $[M + H]^+$. Crystals of **1**·0.5H_2O (Fig. 1) suitable for X-ray diffraction analysis were obtained by recrystallization of compound **1** from EtOH solution. Crystal data for $C_{14}H_{19}N_6O_{2.5}$: crystal size: 0.45 × 0.17 × 0.15 mm, orthorhombic, space group *Pbca*. a = 18.204(19) Å, b = 15.339(15) Å, c = 23.87(2) Å, V = 6666(11) Å^3, Z = 16, T = 296(2) K, θ = 1.71–25.00°, 31 591 reflections measured, 5856 unique (R_{int} = 0.1615). Final residual for 415 parameters and 5856 reflections with $I > 2\sigma(I)$: R_1 = 0.0711, wR_2 = 0.1843 and GOF = 1.040.

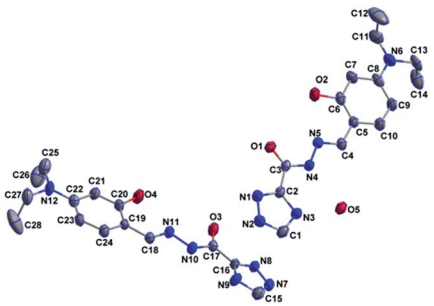

Fig. 1 Crystal structure of **1**·0.5H_2O.

General UV-vis and fluorescence spectra measurements

The spectral analyses were accomplished in buffered CH_3CN/HEPES (10 mM, 1/1, v/v, pH = 6.0 and or 10.0 for the detection of Al^{3+}/Cu^{2+} and Zn^{2+}, respectively) solution at room temperature. The concentration of the probe **1** for UV-vis and fluorescence measurement was 5 μM. Nitrate salts of different cations (Ag^+, Al^{3+}, Ca^{2+}, Cd^{2+}, Co^{2+}, Cr^{3+}, Cu^{2+}, Fe^{3+}, Hg^{2+}, K^+, Mg^{2+}, Mn^{2+}, Na^+, Ni^{2+}, Pb^{2+}, and Zn^{2+}) and sodium or ammonium salts of different anions (AcO^-, F^-, Cl^-, Br^-, I^-, CN^-, SCN^-, N_3^-, ClO_4^-, HSO_4^-, HSO_3^-, $H_2PO_4^-$, HPO_4^{2-}, S^{2-} and PO_4^{3-}) were used for different titration experiments. UV-vis and fluorescence spectrophotometric titration were conducted directly in 2 mL cuvette by successive addition of corresponding chemical reagent using a microliter syringe. Upon addition of every aliquot, the solution was well mixed then the spectrum was measured.

Results and discussions

UV-vis spectroscopic studies of 1 with metal ions in buffered CH_3CN/HEPES solution (10 mM, 1/1, v/v) at pH 6.0

The UV-vis spectrum of probe **1** (5 μM) in buffered CH_3CN/HEPES solution (10 mM, 1/1 v/v, pH 6.0) features only one band centered at 376 nm, which should be assigned to the π–π* transition of the imine units.[33] Upon addition of metal ions (1 eq.), including Ag^+, Al^{3+}, Ca^{2+}, Cd^{2+}, Co^{2+}, Cr^{3+}, Cu^{2+}, Fe^{3+}, Hg^{2+}, K^+, Mg^{2+}, Mn^{2+}, Na^+, Ni^{2+}, Pb^{2+}, and Zn^{2+} to the solution of **1**, dramatic change in the UV spectra could be obtained only in the case of Cu^{2+}. As shown in Fig. 2, a ~20 nm redshift selectively for Cu^{2+} was observed, corresponding for the green color. In addition, the presence of the other competitive metal ions did not lead to any significant changes in the absorbance of **1** + Cu^{2+} at 398 nm (Fig. S1, ESI†), thereby establishing that the other metal ions do not interfere with Cu^{2+} detection. As expected, **1** is

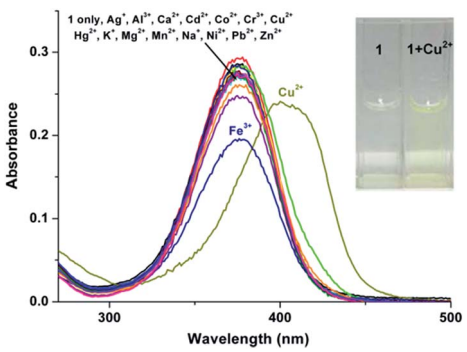

Fig. 2 UV-vis spectra of 5 μM probe **1** in buffered CH_3CN/HEPES solution (10 mM, 1/1, v/v, pH = 6.0) with 1 eq. of metal ions: Ag^+, Al^{3+}, Ca^{2+}, Cd^{2+}, Co^{2+}, Cr^{3+}, Cu^{2+}, Fe^{3+}, Hg^{2+}, K^+, Mg^{2+}, Mn^{2+}, Na^+, Ni^{2+}, Pb^{2+} and Zn^{2+} ions and blank. The insert shows the color of probe **1** only and with the addition of Cu^{2+} ion.

a "naked-eye" colorimetric probe with high selectivity towards Cu^{2+}.

To evaluate the sensing properties of **1** (5 μM) as a receptor, a titration experiment was carried out with gradual addition of Cu^{2+} ions (0–2 eq.). As shown in Fig. 3, the absorbance at 376 nm decreases gradually upon addition of Cu^{2+}, along with a concomitant generation of a new peak at 398 nm. The appearance of the isosbestic point at 390 nm indicates that the coordination reaction is clean and straightforward.[20] In addition, the probe **1** showed a good linear relationship between the absorbance ratio of A_{398}/A_{376} and the concentration of Cu^{2+} ions from 0 to 5 μM (Fig. 3, inset). Thus, sensor **1** is potentially applicable for quantitative analysis of Cu^{2+}. The detection limit of **1** for Cu^{2+} is 106.4 nM, which was calculated using the equation DL = $3S_{bi}/S$ (where S_{bi} is the standard deviation of blank measurements and S is the slope of the intensity *versus* sample concentration).[27] Job's plot experiment result suggests that the binding of **1** to Cu^{2+} is of 1 : 1 stoichiometry (Fig. S2, ESI†). The association constant (K_a) was calculated to be 5.50×10^4 M^{-1} by fitting the data to the Benesi–Hildebrand expression (Fig. S3, ESI†). The probe **1** can function in the pH range of 5.0–12.0 (Fig. S4, ESI†), which is relatively wide when compared to some rhodamine based Cu^{2+} ion chemosensors.[34,35]

Fluorescence spectroscopic studies of 1 with metal ions in buffered CH_3CN/HEPES solution (10 mM, 1/1, v/v) at pH 6.0

As shown in Fig. 4, excitation of **1** (5 μM) at 390 nm in buffered CH_3CN/HEPES solution (10 mM, 1/1, v/v) at pH 6.0 shows weak emission at 460 nm (the pass width of emission and excitation being 2.5 nm). Addition of Al^{3+} to **1** solution induces a significant fluorescence enhancement (light-blue emission under 365 nm UV lamp, Fig. 4, inset). By contrast, the addition of the other metal ions does not lead to any noticeable spectral change (except for Zn^{2+}, which showed a slight fluorescence enhancement). In addition, the fluorescence of the **1** + Al^{3+} complex could be maintained in the presence of most of the other metal ions (Fig. S5, ESI,† except for Cu^{2+}, because of its inherent magnetic property; and Cr^{3+}, probably due to its strong Lewis acidity, resulting in the hydrolytic cleavage of the imine bond[36]).

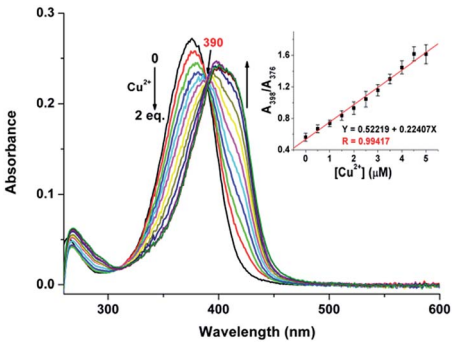

Fig. 3 Absorption spectra of 5 μM probe **1** upon the addition of Cu^{2+} (0–2 eq.) in buffered CH_3CN/HEPES solution (10 mM, 1/1, v/v, pH = 6.0). The inset shows the absorbance ratio of A_{398}/A_{376} as a function of Cu^{2+} concentration (0–5 μM).

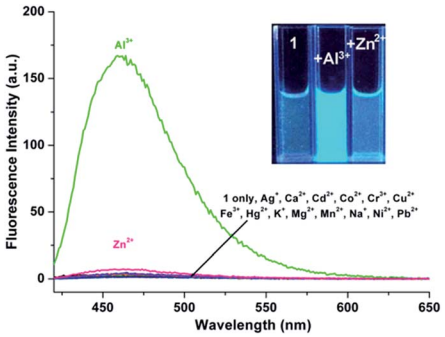

Fig. 4 Fluorescence emission spectra of 5 μM probe **1** in buffered CH_3CN/HEPES solution (10 mM, 1/1, v/v, pH = 6.0) with 1 eq. of metal ions: Ag^+, Al^{3+}, Ca^{2+}, Cd^{2+}, Co^{2+}, Cr^{3+}, Cu^{2+}, Fe^{3+}, Hg^{2+}, K^+, Mg^{2+}, Mn^{2+}, Na^+, Ni^{2+}, Pb^{2+} and Zn^{2+} ions and blank, excitation wavelength was 390 nm (the pass width of emission and excitation being 2.5 nm). The insert shows the change of the color of probe **1** only and with the addition of Al^{3+} and Zn^{2+} under 365 nm UV lamp, respectively.

The titration experiment of the probe with increasing concentration of Al^{3+} (Fig. 5) showed that the fluorescence intensity at 460 nm of a 5 μM solution of **1** increased linearly with incremental addition of Al^{3+} ions (1–6.5 μM). The detection limit of **1** for Al^{3+} is calculated to be 22.5 nM. The quantum yields of the solutions of **1** (5 μM) with and without 1 eq. Al^{3+} ions are 0.28 and 0.02, respectively, using quinine sulfate as standard (Φ_F = 0.546 in 0.5 mol L^{-1} H_2SO_4).[20] Furthermore, Job's plot experiment shows that the binding of **1** to Al^{3+} is of 1 : 1 stoichiometry (Fig. S6, ESI†), whose association constant (K_a) was calculated to be 1.01×10^5 M^{-1} (Fig. S7, ESI†).

Fluorescence spectroscopic studies of 1 with metal ions in buffered CH_3CN/HEPES solution (10 mM, 1/1, v/v) at pH 10.0

During the experimental process, we found that the fluorescence intensity of the solution of **1** may be enhanced by adding Zn^{2+} to certain amount. Therefore, CH_3CN/HEPES solution (10 mM, 1/1, v/v) at pH 10.0 was employed as a tested media to

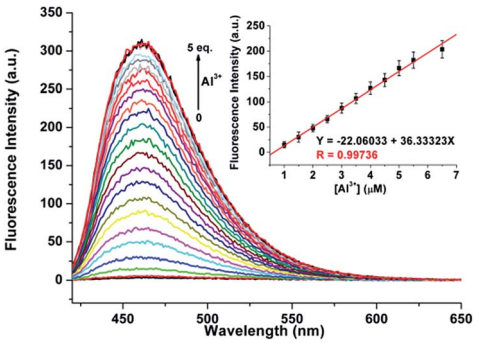

Fig. 5 Fluorescence emission spectra of 5 μM probe **1** upon the addition of Al^{3+} (0–5 eq.) in buffered CH_3CN/HEPES solution (10 mM, 1/1, v/v, pH = 6.0). The inset shows the fluorescence intensities at 460 nm as a function of Al^{3+} concentration (1–6.5 μM). Excitation wavelength was 390 nm (the pass width of emission and excitation being 2.5 nm).

detect Zn^{2+} ion (the pass width of emission and excitation being 5 nm). It is observed that only the presence of Zn^{2+} ions induces clear fluorescent enhancement of **1** (Fig. 6), which indicates the high selectivity of probe **1** for Zn^{2+} ion. Unfortunately, several transition metal ions, such as Ag^{+}, Al^{3+}, Co^{2+}, Cu^{2+}, Hg^{2+}, Mn^{2+}, and Ni^{2+} ions could interfere with the Zn^{2+} detection (Fig. S8, ESI†). The titration experiment shows that the fluorescence intensity at 470 nm increased linearly over the Zn^{2+} concentration range of 0.5–4 μ M (Fig. 7). The detection limit of **1** for Zn^{2+} is 102.5 nM, which is sufficiently low for Zn^{2+} detection in many chemical and biological systems.[20]

The spectral response of **1** (5 μM) with or without Al^{3+}/Zn^{2+} (1 eq.) in CH_3CN/HEPES (v/v = 1 : 1) solution at different pH values was evaluated at room temperature. As shown in Fig. S9 and S10, ESI,† the sensor **1** can detect Al^{3+} ions in the pH range of 4.0–8.0, while 7.0–12.0 in the case of Zn^{2+} detection. All results show that sensor **1** may be used as a candidate for detecting Al^{3+} and Zn^{2+} in semi-aqueous media.

Spectroscopic studies of the 1 + Al^{3+} system in the presence of F^{-} ions

The advantage of the reversibility of the probe based on coordination reaction (*vide infra*) was taken into consideration.[30] The rupture of the **1** + Al^{3+} species to regenerate **1**, and the subsequent change in the optical properties of **1** + Al^{3+} system in buffered CH_3CN/HEPES solution (10 mM, 1/1, v/v) at pH 6.0, were studied by introducing a variety of anions (AcO^{-}, F^{-}, Cl^{-}, Br^{-}, I^{-}, CN^{-}, SCN^{-}, N_3^{-}, ClO_4^{-}, HSO_4^{-}, HSO_3^{-}, $H_2PO_4^{-}$, HPO_4^{2-}, S^{2-} and PO_4^{3-}). The significant quenching of fluorescence in the **1** + Al^{3+} system due to regeneration of **1** was observed only in the presence of F^{-} ions (Fig. 8, the pass width of emission and excitation being 2.5 and 5 nm, respectively). In addition, the presence of competitive anions do not interfere with F^{-} detection (Fig. S11, ESI†). It is suggested that the strong interaction of Al^{3+} and F^{-} ions possibly facilitates the rupture of the **1** + Al^{3+} complex in support of a quenching phenomenon, by the reduction in fluorescence intensity at 460 nm, which is also supported by UV spectrum (Fig. S12, ESI†). The titration experiment (Fig. 9) showed that the fluorescence intensity at 460 nm of **1** + Al^{3+} system decreased linearly with gradual addition of F^{-} ions (1–10 μM). Based on the above fluorescence titration analysis, the detection limit is found to be 30.6 nM, which is quite lower than some of the reported resultant metal-probe complex sensors for F^{-} ions.[25] Reaction mechanism of **1** with Cu^{2+}, Al^{3+} and Zn^{2+}. The reaction mechanism of **1** with Cu^{2+}, Al^{3+}, and Zn^{2+} was explored using ESI-MS analysis. The ESI-MS spectra of **1** + Cu^{2+}, **1** + Al^{3+}, and **1** + Zn^{2+} exhibit peaks at *m*/*z* 363.0863, 390.1046, and 406.0924 (Fig S13–S15, ESI†), which should be assigned to [Cu(1-2H)], [Al(1-2H)(NO_3)], and [Zn(1-2H)(CH_3CN)], respectively. Moreover, the ^1H NMR spectral differences between **1** and **1** + Al^{3+}/Zn^{2+} is shown in Fig. 10. The proton peaks at 14.79 and 12.13 should be assigned to OH and NH–C=O of **1**, respectively. Both peaks disappeared in the spectra of **1** + Al^{3+} and **1** + Zn^{2+}, confirming the metal binding of the phenolic hydroxyl and the enolizated hydrazone carbonyl

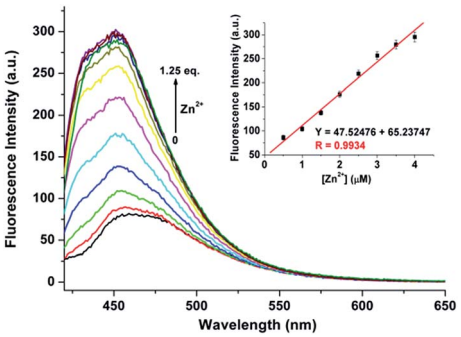

Fig. 7 Fluorescence emission spectra of 5 μM probe **1** upon the addition of Zn^{2+} (0–1.25 eq.) in buffered CH_3CN/HEPES solution (10 mM, 1/1, v/v, pH = 10.0). The inset shows the fluorescence intensities at 460 nm as a function of Zn^{2+} concentration (0.5–4 μM). Excitation wavelength was 390 nm (the pass width of emission and excitation being 5 nm).

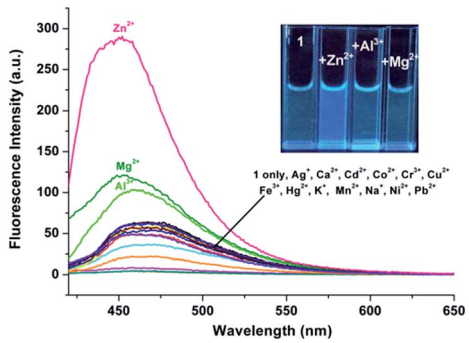

Fig. 6 Fluorescence emission spectra of 5 μM probe **1** in buffered CH_3CN/HEPES solution (10 mM, 1/1, v/v, pH = 10.0) with 1 eq. of metal ions: Ag^{+}, Al^{3+}, Ca^{2+}, Cd^{2+}, Co^{2+}, Cr^{3+}, Cu^{2+}, Fe^{3+}, Hg^{2+}, K^{+}, Mg^{2+}, Mn^{2+}, Na^{+}, Ni^{2+}, Pb^{2+} and Zn^{2+} ions and blank, excitation wavelength was 390 nm (the pass width of emission and excitation being 5 nm). The insert shows the change of the color of probe **1** only and with the addition of Al^{3+}, Mg^{2+}, and Zn^{2+} under 365 nm UV lamp, respectively.

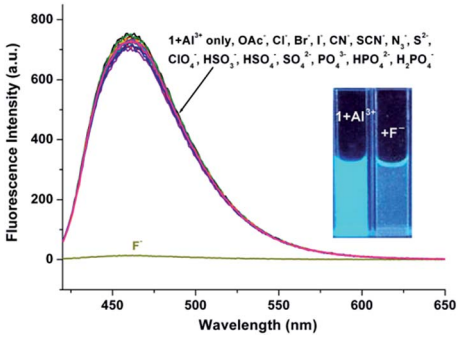

Fig. 8 Fluorescence emission spectra of 5 μM probe **1** + Al^{3+} (1 eq.) in buffered CH_3CN/HEPES solution (10 mM, 1/1, v/v, pH = 6.0) with 10 eq. of common anions: AcO^{-}, F^{-}, Cl^{-}, Br^{-}, I^{-}, CN^{-}, SCN^{-}, N_3^{-}, ClO_4^{-}, HSO_4^{-}, HSO_3^{-}, $H_2PO_4^{-}$, HPO_4^{2-}, S^{2-}, PO_4^{3-}, and blank, excitation wavelength was 390 nm (the pass width of emission and excitation being 2.5 and 5 nm, respectively). The insert shows the change of the color of **1** + Al^{3+} only and with the addition of F^{-} under 365 nm UV lamp.

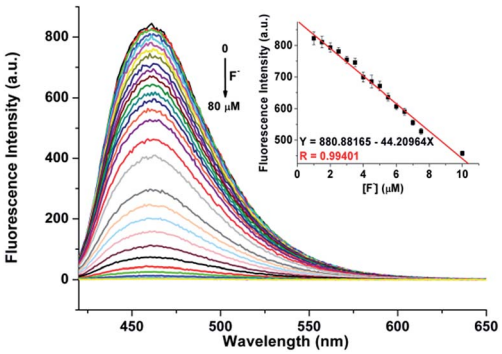

Fig. 9 Fluorescence emission spectra of 5 μM probe **1** + Al^{3+} (1 eq.) upon the addition of F^- (0–80 μM) in buffered CH_3CN/HEPES solution (10 mM, 1/1, v/v, pH = 6.0). The inset shows the fluorescence intensities at 460 nm as a function of F^- concentration (0–4 μM). Excitation wavelength was 390 nm (the pass width of emission and excitation being 2.5 and 5 nm, respectively).

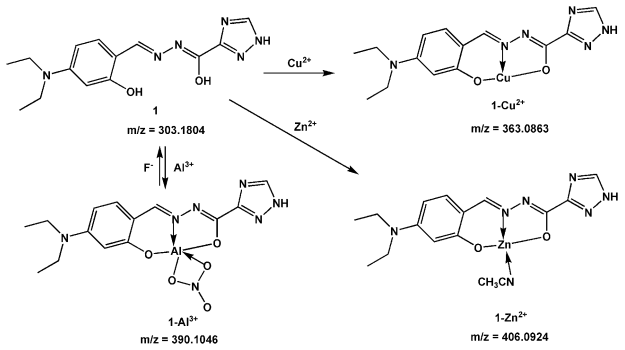

Scheme 2 The proposed reaction mechanism of **1** with Cu^{2+}, Al^{3+}, and Zn^{2+} ions.

groups. Although the CH=N signal gives almost no shift, the triazole NH of **1** shifts to lower field in the presence of Al^{3+}/Zn^{2+}, probably due to the coordination of imine N atom according to the previous results.[37] Therefore, it is suggested that **1** could chelate metal ions (such as Cu^{2+}, Al^{3+}, and Zn^{2+}) to form 1 : 1 complex with O_2N donor set (Scheme 2).

To further clarify the configuration of **1** and corresponding complexes, we performed density functional theory (DFT) calculations with the Becke-3–Lee–Yang–Parr (B3LYP) exchange function using the Gaussian 09 package.[38] Results show that probe **1** adopts a 1 : 1 binding stoichiometry with Cu^{2+}, Zn^{2+}, and Al^{3+} ions (Fig. 11). In all three complexes, **1** uses the N atom of imine and two deprotonated O atoms of both hydroxyl and enolized carboxyl groups to coordinate with metal ions (an additional coordinated CH_3CN molecule for Zn^{2+}, whereas a bidentate nitrate anion in the case of Al^{3+}), thus acting as a tridentate dianionic ligand. The coordination bond lengths of **1**-Cu^{2+}, **1**-Zn^{2+} and **1**-Al^{3+} range from 1.833–1.947, 1.944–2.179, and 1.775–1.973 Å, respectively. As shown in Scheme 3, the free Schiff base sensor **1** displayed weak fluorescence emission primarily due to the C=N isomerization. Binding with Zn^{2+}/Al^{3+} ions inhibits the isomerization of C=N, thus enhancing the fluorescence intensity through the chelation-enhanced fluorescence (CHEF) mechanism.[39]

The spatial distributions and orbital energies of the HOMO and LUMO of **1**, **1**-Cu^{2+}, **1**-Al^{3+}, and **1**-Zn^{2+} complexes were also generated (Fig. 11). The 3D isosurface HOMO and LUMO diagram showed that the electron densities of HOMOs for four compounds are more or less similar, and mostly located on the probe moiety, whereas those of LUMOs are separated to the coordination solvent (for **1**-Zn^{2+}) or anion (for **1** + Al^{3+}). Both HOMO and LUMO of **1**-Cu^{2+} are concerned with the metal ion, clearly establishing the charge transfer process from probe **1** to Cu^{2+} ion. In addition, LUMO and HOMO energies are calculated to be −1.38 eV and −5.07 eV, respectively, for probe **1**. In **1**-Cu^{2+}, **1**-Zn^{2+}, and **1**-Al^{3+} complexes, the respective LUMO and HOMO energies are −1.61 and −5.23 eV, −0.95 and −4.51 eV, −2.14 and −5.55 eV, respectively. The corresponding energy difference ΔE of **1**, **1**-Cu^{2+}, **1**-Zn^{2+}, and **1**-Al^{3+} are 3.69, 3.62, 3.56 and 3.41 eV, respectively, suggesting that the complexes are more stable than the free probe **1**.

Fluorescence imaging of intercellular Al^{3+}, Zn^{2+} and F^-

The ability of the fluorescence chemosensor **1** to detect Al^{3+}, Zn^{2+} and F^- in Hela cells was examined. The cells were added with **1** (5 μM) in Dulbecco's modified Eagle's medium (DMEM) supplemented with 10% fetal bovine serum for 30 min at 37 °C,

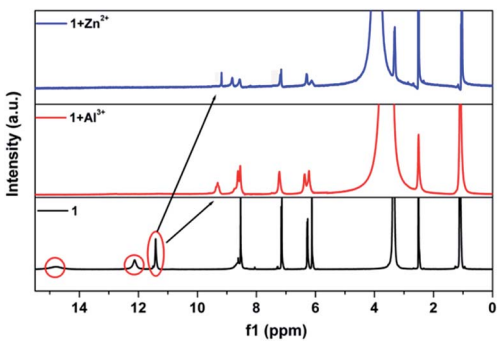

Fig. 10 ^1H NMR spectral changes of **1** with the addition of Al^{3+}/Zn^{2+} in DMSO-d_6 solution.

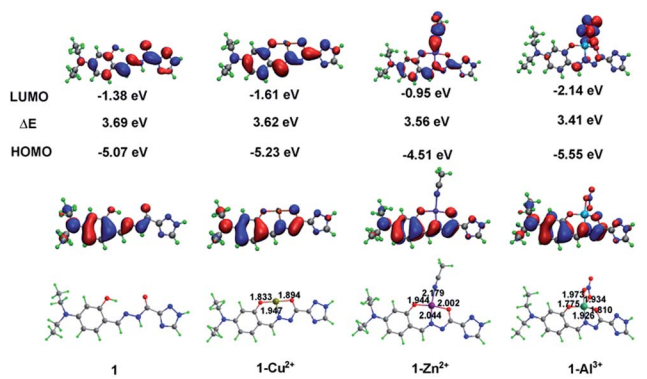

Fig. 11 Optimized structures and HOMO/LUMO of **1**, complexes **1**-Cu^{2+}, **1**-Al^{3+} and **1**-Zn^{2+} by DFT calculation.

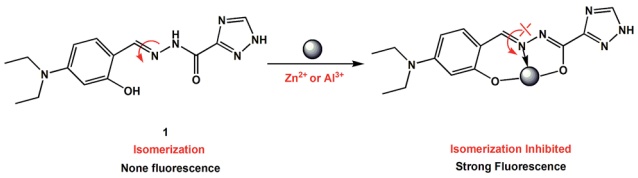

Scheme 3 Possible luminescence mechanism of **1** with Al^{3+}/Zn^{2+}.

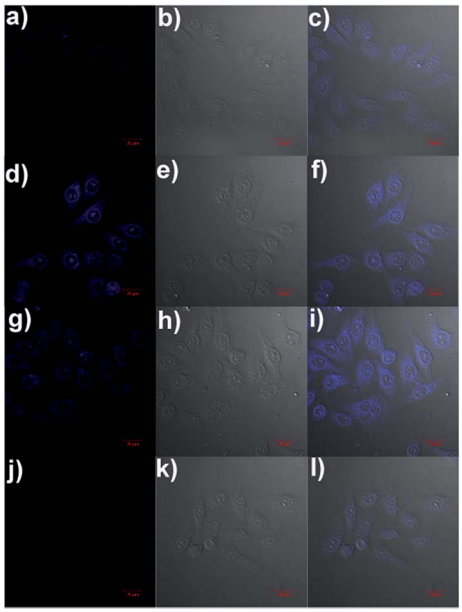

Fig. 12 Confocal fluorescence images of HeLa cells: confocal fluorescence (a), brightfield (b), and overlay (c) images of HeLa cells incubated with 5 μM of **1** for 30 min at 37 °C; confocal fluorescence (d), brightfield (e), and overlay (f) images of HeLa cells incubated with 5 μM of **1** for 30 min at 37 °C and then incubated with 5 μM Al^{3+} for another 30 min at 37 °C; confocal fluorescence (g), brightfield (h), and overlay (i) images of HeLa cells incubated with 5 μM of **1** for 30 min at 37 °C and then incubated with 5 μM Zn^{2+} for another 30 min at 37 °C; confocal fluorescence (j), brightfield (k), and overlay (l) images of HeLa cells incubated with 5 μM of **1** and Al^{3+} (5 μM) for 30 min at 37 °C and then incubated with 20 μM F^- for another 30 min at 37 °C.

leading to weak intracellular fluorescence as determined by laser scanning confocal microscopy (Fig. 12a). Free **1** was removed by rinsing the cells with DMEM. Then the cells were added with 5 μM Al^{3+}/Zn^{2+} in DMEM supplemented with 10% fetal bovine serum and incubated for another 30 min at 37 °C under same imaging condition. A significant increase in the fluorescence from the intracellular area was observed (Fig. 12d and g). In addition, the cells supplemented with **1** and Al^{3+} were further treated with F^- (20 μM), the strong intracellular fluorescence became weak (Fig. 12j). All facts suggest that sensor **1** can be used to image intracellular Al^{3+}, Zn^{2+} and F^- in living cells.

Conclusion

In summary, a simple Schiff base has been presented as a fluorescent off–on sensor for Al^{3+} and Zn^{2+} under different pH conditions, as well as a colorimetric probe for Cu^{2+} in semi-aqueous media. The sensor functions by forming stable complexes with $Cu^{2+}/Zn^{2+}/Al^{3+}$, and the detection limit of the sensor is at the parts per million level for each of the metal ions. In addition, the resultant **1** + Al^{3+} complex could act as an 'on–off' fluorescent sensor for F^-. The probe **1** was also used to determine Al^{3+}, Zn^{2+} and F^- in living cells.

Conflicts of interest

There are no conflicts to declare.

Acknowledgements

This work was supported in part by the National Natural Science Foundation of China (No. 21001040), the Joint Program for Fostering Talents of National Natural Science Foundation of China and Henan Province (U1304202 and U1604124), the Science and Technology Department of Henan Province (162300410011, 162300410236, 152102210343 and 152102210314), the Education Department of Henan Province (No. 15B150016 and 15HASTIT002), and Outstanding Youth Funds of Henan Polytechnic University (J2015-4).

Notes and references

1 Y. Yang, Q. Zhao, W. Feng and F. Li, *Chem. Rev.*, 2013, **113**, 192.
2 K. P. Carter, A. M. Young and A. E. Palmer, *Chem. Rev.*, 2014, **114**, 4564.
3 Z. Liu, C. Peng, Z. Lu, X. Yang, M. Pei and G. Zhang, *Dyes Pigm.*, 2015, **123**, 85.
4 A. Liu, L. Yang, Z. Zhang, Z. Zhang and D. Xu, *Dyes Pigm.*, 2013, **99**, 472.
5 W. Cao, X. J. Zheng, J. P. Sun, W. T. Wong, D. C. Fang, J. X. Zhang and L. P. Jin, *Inorg. Chem.*, 2014, **53**, 3012.
6 Y. W. Choi, G. J. Park, Y. J. Na, H. Y. Jo, S. A. Lee, G. R. You and C. Kim, *Sens. Actuators, B*, 2014, **194**, 343.
7 S. K. Sheet, B. Sen, R. Thounaojam, K. Aguan and S. Khatua, *J. Photochem. Photobiol., A*, 2017, **332**, 101.
8 C.-R. Li, J.-C. Qin, B.-D. Wang, X. Bai and Z.-Y. Yang, *J. Photochem. Photobiol., A*, 2017, **332**, 141.
9 H. Wang, B. Wang, Z. Shi, X. Tang, W. Dou, Q. Han, Y. Zhang and W. Liu, *Biosens. Bioelectron.*, 2015, **65**, 91.
10 P. Li and S. Xiao, *J. Photochem. Photobiol., A*, 2016, **330**, 169.
11 C. Liang, W. Bu, C. Li, G. Men, M. Deng, Y. Jiangyao, H. Sun and S. Jiang, *Dalton Trans.*, 2015, **44**, 11352.
12 N. R. Chereddy, M. V. N. Raju, B. M. Reddy, V. R. Krishnaswamy, P. S. Korrapati, B. J. M. Reddy and V. J. Rao, *Sens. Actuators, B*, 2016, **237**, 605.
13 J. Li, C. Yin and F. Huo, *Dyes Pigm.*, 2016, **131**, 100.
14 X. Chen, T. Pradhan, F. Wang, J. S. Kim and J. Yoon, *Chem. Rev.*, 2012, **112**, 1910.
15 Y. Zhou, Z.-X. Li, S.-Q. Zang, Y.-Y. Zhu, H.-Y. Zhang, H.-W. Hou and T. C. W. Mak, *Org. Lett.*, 2012, **14**, 1214.
16 K. P. Carter, A. M. Young and A. E. Palmer, *Chem. Rev.*, 2014, **114**, 4564.

17 C. Chen, G. Men, W. Bu, C. Liang, H. Sun and S. Jiang, *Sens. Actuators, B*, 2015, **220**, 463.
18 K. Ponnuvel, M. Kumar and V. Padmini, *Sens. Actuators, B*, 2016, **227**, 242.
19 W.-K. Dong, X.-L. Li, L. Wang, Y. Zhang and Y.-J. Ding, *Sens. Actuators, B*, 2016, **229**, 370.
20 W. N. Wu, P. D. Mao, L. Jia, Y. Wang and Z. Q. Xu, *Spectrochim. Acta, Part A*, 2016, **166**, 44.
21 Y. Wang, H.-Q. Chang, W.-N. Wu, W.-B. Peng, Y.-F. Yan, C.-M. He, T.-T. Chen, X.-L. Zhao and Z.-Q. Xu, *Sens. Actuators, B*, 2016, **228**, 395.
22 J.-J. Xiong, P.-C. Huang, C.-Y. Zhang and F.-Y. Wu, *Sens. Actuators, B*, 2016, **226**, 30.
23 C. Parthiban, S. Ciattini, L. Chelazzi and K. P. Elango, *Sens. Actuators, B*, 2016, **231**, 768.
24 S. Nandi and D. Das, *ACS Sens.*, 2016, **1**, 81.
25 H. Liu, B. Zhang, C. Tan, F. Liu, J. Cao, Y. Tan and Y. Jiang, *Talanta*, 2016, **161**, 309.
26 Y. Tang, J. Sun and B. Yin, *Anal. Chim. Acta*, 2016, **942**, 104.
27 V. K. Gupta, N. Mergu and L. K. Kumawat, *Sens. Actuators, B*, 2016, **223**, 101.
28 X. Shi, W. Fan, C. Fan, Z. Lu, Q. Bo, Z. Wang, C. A. Black, F. Wang and Y. Wang, *Dyes Pigm.*, 2017, **140**, 109.
29 B. Sen, M. Mukherjee, S. Banerjee, S. Pal and P. Chattopadhyay, *Dalton Trans.*, 2015, **44**, 8708.
30 A. Roy, S. Dey and P. Roy, *Sens. Actuators, B*, 2016, **237**, 628.
31 G. M. Sheldrick, *SADABS*, University of Göttingen, Germany, 1996.
32 G. M. Sheldrick, *SHELX-97, Program for the Solution and the Refinement of Crystal Structures*, University of Göttingen, Germany, 1997.
33 Neeraj, A. Kumar, S. K. Asthana, Shweta and K. K. Upadhyay, *J. Photochem. Photobiol., A*, 2016, **329**, 69.
34 R. R. Nair, M. Raju, N. P. Patel, I. H. Raval, E. Suresh, S. Haldar and P. B. Chatterjee, *Analyst*, 2015, **140**, 5464.
35 S. Pal, B. Sen, S. Lohar, M. Mukherjee, S. Banerjee and P. Chattopadhyay, *Dalton Trans.*, 2015, **44**, 1761.
36 J.-C. Qin, L. Fan and Z.-Y. Yang, *Sens. Actuators, B*, 2016, **228**, 156.
37 C. Patra, A. K. Bhanja, C. Sen, D. Ojha, D. Chattopadhyay, A. Mahapatra and C. Sinha, *Sens. Actuators, B*, 2016, **228**, 287.
38 M. J. Frisch, G. W. Trucks, H. B. Schlegel, G. E. Scuseria, M. A. Robb and J. R. Cheeseman, *et al.*, *Gaussian 09, Revision D.01,Gaussian, Inc.*, Wallingford CT, 2013.
39 D. Pratap Singh and V. P. Singh, *J. Lumin.*, 2014, **155**, 7.

